Realization of the high-performance THz GaAs homojunction detector below the frequency of Reststrahlen band

Peng Bai,[1,2] Y. H. Zhang,[1,2,a)] X. G. Guo,[3] Z. L. Fu,[4] J. C. Cao,[4] and W. Z. Shen[1,2]
[1]*Key Laboratory of Artificial Structures and Quantum Control, School of Physics and Astronomy, Shanghai Jiao Tong University, Shanghai 200240, China*
[2]*Collaborative Innovation Center of Advanced Microstructures, Nanjing 210093, China*
[3]*School of Optical-Electrical and Computer Engineering, University of Shanghai for Science and Technology, Shanghai 200093, China*
[4]*Key Laboratory of Terahertz Solid-State Technology, Shanghai Institute of Microsystem and Information Technology, Chinese Academy of Sciences, Shanghai 200050, China*

(Received 22 September 2018; accepted 23 November 2018; published online 12 December 2018)

High-performance terahertz (THz) detectors are in great need in the applications of security, medicine, as well as in astronomy. A high responsivity p-GaAs homojunction interfacial workfunction internal photoemission (HIWIP) detector was demonstrated for a specific frequency (5 THz) below the frequency of the Reststrahlen band. The experimental results indicate that the optimized detector shows significant enhancement of the response below the Reststrahlen band in contrast to the conventional detectors. With the bottom gold layer serving as a perfect reflector, nearly 50% increment of responsivity and quantum efficiency was obtained further due to the cavity effect. Though very simple, such reflector design shows a satisfactory effect and is easy to be realized in practical applications. The resultant peak responsivity of the detector with a bottom reflector could be as high as 6.8 A/W at 1 V bias. The noise equivalent power is $2.3 \times 10^{-12}\,\mathrm{W/Hz^{1/2}}$. Due to the absorption ability to normal incident light and high responsivity, the p-GaAs HIWIP detector is promising for the focal plane array and large-scale pixelless imaging applications. *Published by AIP Publishing.*
https://doi.org/10.1063/1.5061696

Terahertz (THz) detectors have gained more attention and been intensively explored recently, thanks to their numerous applications in security, medicine, biology, astronomy, and non-destructive materials testing.[1,2] In view of the availability of the mature material and processing technology, GaAs-based detectors are widely used for THz detection. However, strong absorption by the optical phonons of GaAs causes a dark region in 32–36 meV (7.8–8.7 THz), which is known as the Reststrahlen band and limits the photon detection in this region.[3,4] Moreover, the frequency of most of the state-of-the art THz sources is in the region below the frequency of the Reststrahlen band of GaAs.[5] Therefore, it will be more meaningful to make a study of GaAs-based THz detectors below the Reststrahlen band for practical applications.

As a natural extension of traditional infrared (IR) quantum well photodetectors (QWPs), THz QWP is a formidable competitor benefiting from its rapid intrinsic response speed and flexible wavelength coverage.[3,4,6] However, according to the intersubband transition (ISBT) selection rule, only light polarized in epitaxial growth direction can lead to the absorption of n-type QWPs. This feature requires an extra grating design for the THz QWPs in practical applications, which makes the device fabrication complicated and increases the extra cost.[7,8] An innovation of the THz QWP was reported in 2015, in which an antenna-coupled microcavity geometry was adopted.[9,10] The responsivity for this complicated structure QWIP was greatly improved to ∼5 A/W due to the antenna gain and the microcavity effect. However, the high cost of the double-metal cavity structure may be a huge challenge for large scale applications. Another promising candidate is the quantum dot-in-well infrared photodetector (DWELL) based on p-type intersubband transition. This has been recently demonstrated to exhibit a THz response up to 4.28 THz at high temperatures (100 K–130 K) with normal incidence.[11] Unfortunately, the responsivity of the DWELL in the THz range is only at the level of ∼mA/W.

The detector based on the concept of homo-junction interfacial workfunction internal photoemission (HIWIP) has been a competitive detector for THz detection because of its wide spectrum response coverage, clear physical mechanism and tailorable cutoff frequency (f_c).[12] Compared with QWPs, the greatest advantage of HIWIP is that it allows normal incidence absorption, which provides significant simplification in the fabrication of a large focal plane array.[12] In the past 20 years, both of p-type and n-type GaAs HIWIP detectors have been achieved.[13–17] And, almost all of the detectors showed higher responsivity (>1 A/W) and detectivity than QWIPs (edge coupled and grating coupled) or DWELL detectors (<0.2 mA/W) in the THz band. But even so, the performance is still required to be further improved as possible. High responsivity is helpful to increase the operation temperature which limits the practical application for most of the semiconductor THz detectors. Several theoretical studies show significant improvement of the quantum efficiency (η) due to the cavity effect, if a pair of reflectors or a bottom reflector (BR) is applied to the n-GaAs HIWIP detector.[18,19] However, direct experimental support has not been given till now.

In this paper, we demonstrate a high-performance p-GaAs HIWIP detector for a peak specific frequency (5 THz) below the frequency of the Reststrahlen band. First, the

a)E-mail: yuehzhang@sjtu.edu.cn

Fresnel matrix method was used to optimize the structural parameters. Then, the detector was grown and fabricated accordingly. The optimized detector shows significant enhancement of the response below the Reststrahlen band compared with the conventional detector. Finally, in order to further improve the η, extra light propagating to the substrate is utilized with a reflector formed by a gold layer evaporated to the bottom of the device. Though very simple, such a cavity structure shows a satisfactory effect and leads to $\sim$50% further enhancement of the responsivity and η, which gives direct experimental support of the cavity effect in the THz range.

The structural diagram of the p-GaAs HIWIP detector is shown in Fig. 1(a). From the top to the bottom of the mesa, the function layers are the top metal electrode, the top contact layer, the top emitter layer, periods of emitter/intrinsic layers, the bottom intrinsic layer and the bottom contact layer. A window opens on the top side for front-side illumination. The basic structure is the multi-period emitter/intrinsic layer, where the emitter layers are highly doped. The detection mechanism of the p-GaAs HIWIP detector is shown in Fig. 1(b). Free carrier absorption of infrared radiation occurs in the highly doped emitter layers followed by the internal photoemission of photoexcited carriers. Then, the photoexcited carriers across the intrinsic barrier are collected under an electric field (see supplementary material).

To obtain a high-performance p-GaAs HIWIP detector, optimal parameters are needed. The range of the spectral response for p-GaAs is restricted by the activation energy (Δ).[13] According to the high density (HD) theory,[12,14] the calculated relation of ΔE_v (difference in the valence band edge between the emitter layer and the intrinsic layer), E_F(Fermi level), Δ, λ_c with the doping concentration at $V_b = 20\,\mathrm{mV}$, $T = 4.2\,\mathrm{K}$ is shown in Fig. 1(c). However, the light–heavy hole transition effect[20] reveals that the HD theory will become invalid at high doping levels [$>2 \times 10^{19}\,\mathrm{cm}^{-3}$, the dashed area in Fig. 1(c)]. Thus, we choose $N_d = 1 \times 10^{19}\,\mathrm{cm}^{-3}$, corresponding to the cutoff frequency of $\sim$3.5 THz. The impact ionization theory gives the period number $N \le 21$ as a limit.[17] Therefore, we set the number of multilayer periods as $N = 20$.

According to the detection mechanism of the HIWIP detector,[17] the thicknesses of the emitter layer (d_e) and the intrinsic layer (d_i) would affect the internal photoemission efficiency (η_b) and the collection efficiency (η_c) of the barrier. In addition, d_e and d_i also determine the optical distribution in the active region. The Fresnel matrix method[18,21] was introduced to calculate the light absorption and propagation in the multilayer structure. We set the operation temperature as 4.2 K, the applied bias voltage as $V_b = 20\,\mathrm{mV}$ and the frequency of incident light as 5 THz (60 μm). The calculated relationship of d_e, d_i and η is shown in Fig. 1(d). The η reaches a maximum at $d_e = 17\,\mathrm{nm}$, $d_i = 196\,\mathrm{nm}$.

The wafers were grown according to the optimized device parameters by MBE technology on a semi-insulating substrate. Square mesa structures with various areas from $400 \times 400\,\mu\mathrm{m}^2$ to $1 \times 1\,\mathrm{mm}^2$ were fabricated using optical lithography and wet-chemical etching. An unoptimized

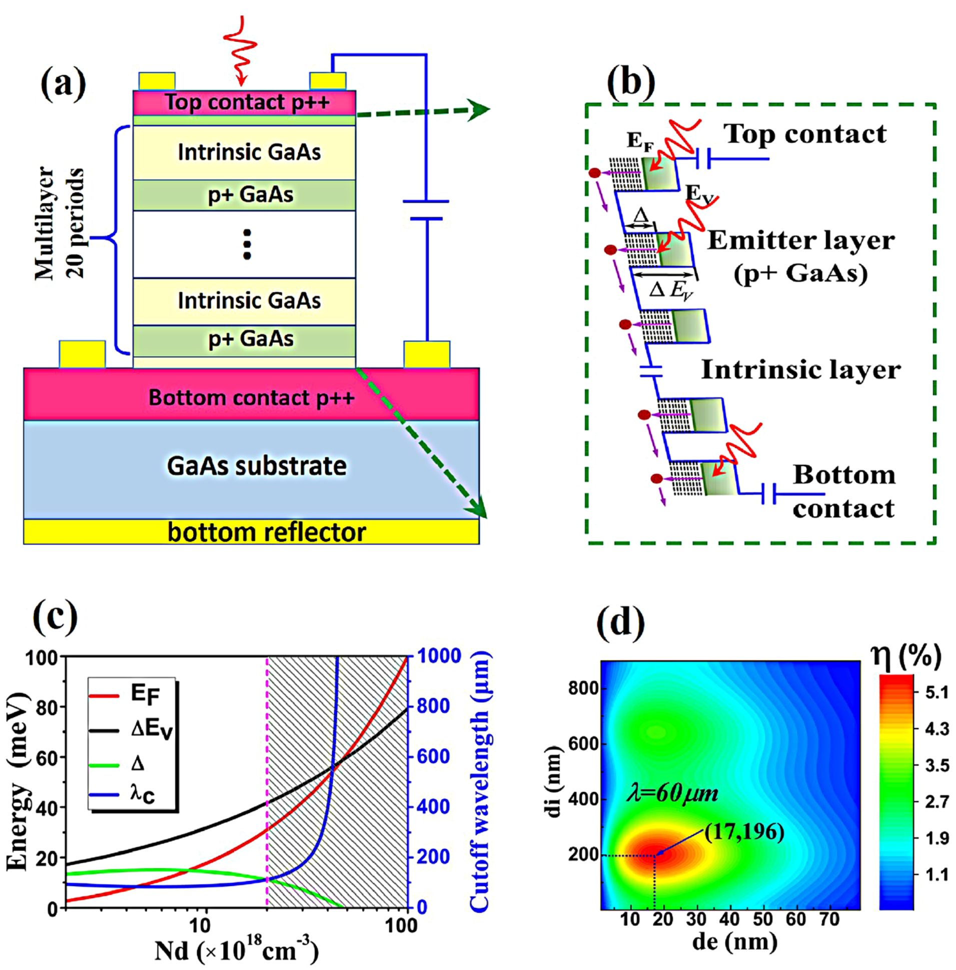

FIG. 1. (a) The structural diagram of the p-GaAs HIWIP detector with BR, (b) the band diagram and the detection mechanism of the p-GaAs HIWIP detector, (c) the calculated concentration dependence of ΔE_v, E_F, Δ, and λ_c at $V_b = 20\,\mathrm{mV}$, $T = 4.2\,\mathrm{K}$, (d) the calculated result of η at different thicknesses of the emitter layer (d_e) and different thicknesses of the intrinsic layer (d_i) of the detector structure without a bottom reflector.

p-GaAs HIWIP detector with a similar cutoff frequency was also fabricated to serve as a reference sample.[17] The cutoff frequency of these two samples is 3.47 THz (optimized) and 3.57 THz (unoptimized), respectively. According to our previous theoretical studies, the efficiency of the HIWIP detector would be improved obviously if a resonant cavity structure is applied.[18,19] In order to make use of the extra light propagating to the substrate and further improve the η, a 100 nm gold layer was evaporated at the back of the device to serve as a reflector and evaluate the cavity effect of the device.

The dark current-voltage characteristics at different temperatures are shown in Fig. 2(a). The dark current (i_d) increases rapidly with increasing temperature for a given bias voltage. The discrepancies at low temperatures are due to different field emission currents caused by different intrinsic layer thicknesses (see supplementary material). The photocurrent spectrum of the optimized detector measured at different bias voltages is shown in Fig. 2(b). The unoptimized detector is also shown in the inset as a reference for comparison. Both

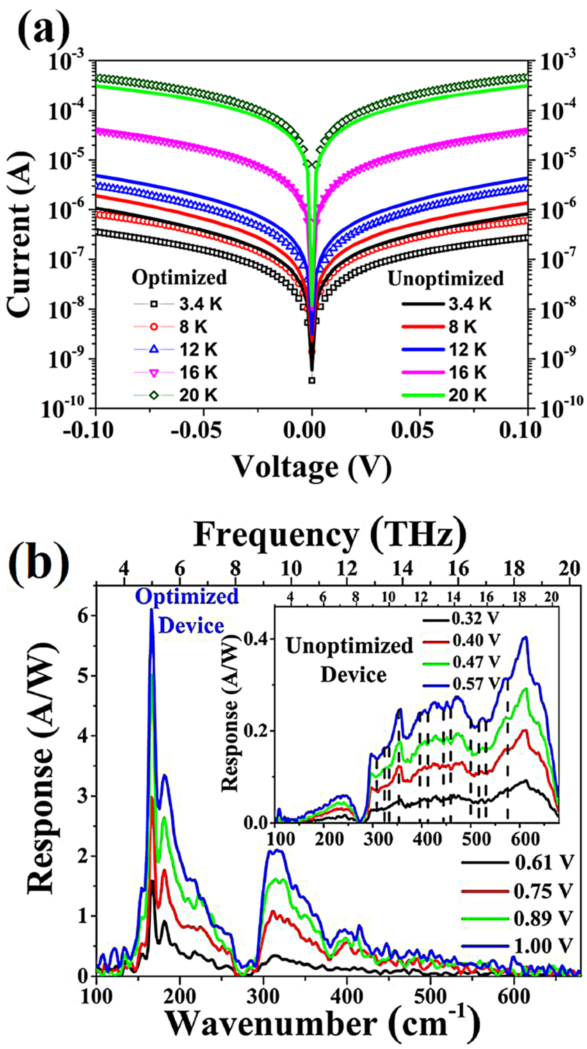

FIG. 2. (a) Experimental dark current of characteristics under different bias voltages. (b) Infrared photocurrent spectrum of the optimized HIWIP detector under different bias voltages (relevant electric fields are about 1.37, 1.68, 1.99, and 2.24 kV/cm, respectively) at 3.4 K. The inset shows the photocurrent spectrum of the unoptimized HIWIP detector under different bias voltages (relevant electric fields are about 1.39, 1.74, 2.04, and 2.48 kV/cm, respectively) at 3.4 K. The vertical dashed lines shown in the inset indicate multiple phonons.[22,23]

of the samples show a strong bias dependence. However, the bias could not be increased infinitely as the dark current increases with the bias and the response will saturate at a high bias.[16] The deep valley between 270 and 300 cm^{-1} corresponds to the transverse optical phonon energy in GaAs (Reststrahlen band). In contrast to the unoptimized detector, the spectral response of the optimized one showed significant enhancement below the Reststrahlen band. The apparent peak frequency (f_P) is below the frequency of the Reststrahlen band, whereas f_P in the unoptimized one and nearly all the other HIWIP-detectors reported before is above the Reststrahlen band. It should be noted that the photo-response of the detector is affected by the optical field distribution, the internal photoemission efficiency η_b and the collection efficiency η_c simultaneously. The improvement in the low frequency region is mainly due to the enhanced optical distribution in the active region. The reduction in the high frequency region is because of the smaller η_b, η_c and the relatively low optical field (see supplementary material). The remarkably reproducible spike response at 5.1 THz (170 cm^{-1}) is from $1s \rightarrow 2p$ transition from impurity absorption of the Be acceptor.[24] This was not observed in the unoptimized one because the response is extremely weak below the Reststrahlen band and 5.1 THz is very close to the cutoff frequency of the detector. Besides, the unoptimized structure may also cause the poor distribution of light in the emitter layer.

Figure 3 shows the experimental variation of the responsivity and η with the bias and the wavenumber for the unoptimized and optimized detectors, respectively. The mesa depth of the optimized detector is about twice that of the unoptimized one. So, the bias voltage applied to the optimized detector should be twice as that of the unoptimized one to ensure the same electric field in the active region. The calibrated responsivity (R) [Fig. 3(a)] and the corresponding η [Fig. 3(b)] of the unoptimized detector show high response above the Reststrahlen band, which agrees with the previous results.[17] The response range above the Reststrahlen band is from 300 cm^{-1} to 680 cm^{-1}, and shows a peak response at 610 cm^{-1}. In contrast, R [Fig. 3(c)] and η [Fig. 3(d)] of the optimized detector show higher photon response efficiency below the Reststrahlen band. R below the Reststrahlen band of the optimized detector is about one order of magnitude higher than that of the unoptimized one under the same electric field, which indicates that the optimized structure not only determined the response frequency of the detector, but also improved the photoresponse efficiency. The remarkable response at 170 cm^{-1} actually resulted from the combined effect of impurity absorption of the Be acceptor and free-carrier absorption of the emitter layer. It should be noted that the impurity absorption of the Be acceptor would not influence our optimization because the general responsivity below the Reststrahlen band itself is higher than that above the Reststrahlen band even without the impurity absorption.

The cavity effect of the device with the BR in the THz region was evaluated by spectral response measurement. Experimental variation of the responsivity (R) and η with the bias and the wavenumber for the detector with BR is shown in Figs. 3(e) and 3(f). The mapping results really show some improvement of photoresponse for the detector with the BR. The resultant peak responsivity of the optimized detector

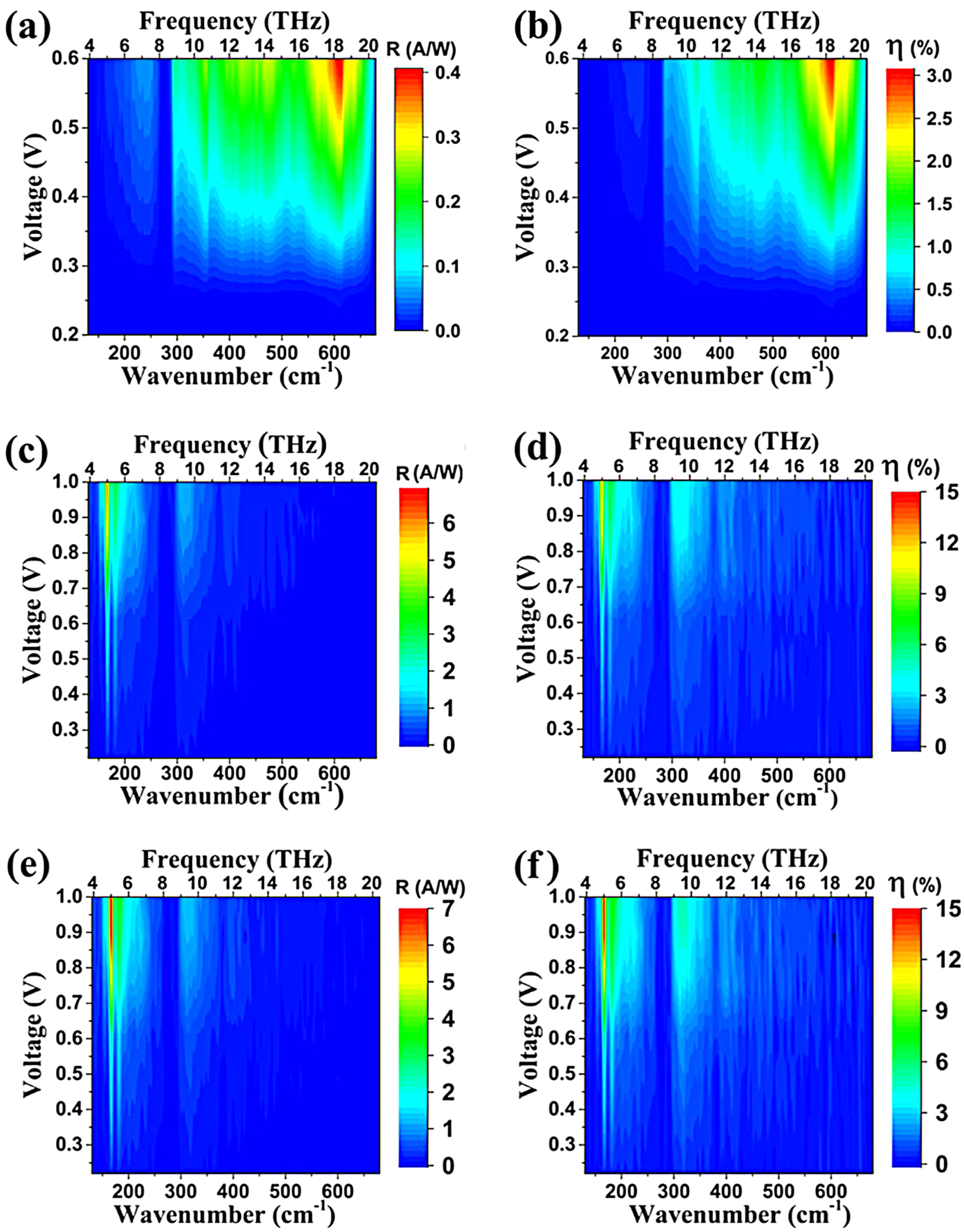

FIG. 3. Variation of (a) and (c) Responsivity and (b) and (d) η ($\eta = h\nu R/q$) with the bias and the wavenumber for the unoptimized and optimized p-GaAs HIWIP detectors, respectively. Also shown are the (e) responsivity and (f) η of the optimized p-GaAs HIWIP detector with BR.

with BR could be as high as 6.8 A/W at 1 V bias. The corresponding η also shows some enhancement compared with the detector without BR. For clarity, R and η at a specific bias voltage (0.61 V) for detectors with BR (red line) and without BR (blue line) are presented in Figs. 4(a) and 4(b). Significant enhancement was achieved for the detector with BR at the same bias voltage. The light travelling to the substrate could be effectively used in the structure with BR. The increment of the η obtained from the experiment is not as obvious as that predicted by the previous theoretical calculation.[19] This may be caused by the absorption of the thick substrate ($\sim$640 μm). Once lapping and polishing the substrate thinner, the R and η of the detector will be much higher. Furthermore, the bias dependent peak responsivity (R_P) and the corresponding NEP ($NEP = i_d/R_P$) for the two detectors (with and without BR) are presented in Fig. 4(c). These results show a maximum improvement of 50% for the responsivity at a bias of 0.61 V. The resultant peak responsivity of the optimized detector with BR could be as high as 6.8 A/W. And, the minimum NEP for the two detectors are 2.3×10^{-12} W/Hz$^{1/2}$ (with BR) and 3×10^{-12} W/Hz$^{1/2}$ (without BR), respectively.

The high-performance p-HIWIP detector can be implemented in a hybridized focal plane array, in which the GaAs substrate is usually completely removed.[25] Beyond that, another potential possible application of the detector is the large area integrated HIWIP-light emitting diode (LED)

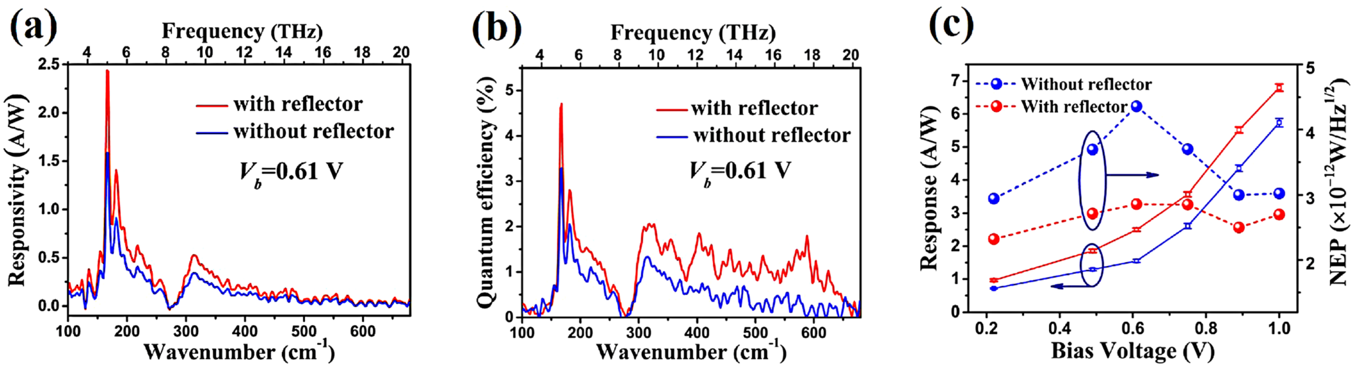

FIG. 4. (a) Responsivity and (b) η of the p-GaAs HIWIP detector with BR (red line) and without BR (blue line). (c) The bias dependent peak responsivity (with error bar) and the corresponding NEP for the two p-GaAs HIWIP detectors (with and without BR).

pixelless imaging devices.[26] The normal incidence absorption simplifies the structure of the HIWIP-LED pixelless imaging devices and makes it more compact. This may have more advantages over the THz QWP-LED, which needs a special design for the grating coupler owing to the intersubband transition selection rule.[27]

In conclusion, we demonstrated a high-performance p-GaAs HIWIP detector for a specific frequency (5 THz) below the Reststrahlen band of GaAs. First, the Fresnel matrix method was used to optimize the structural parameters of the detector. Then, the optimized detector was grown and fabricated accordingly. In contrast to the conventional GaAs HIWIP detectors, the optimized one shows significant enhancement of the response below the Reststrahlen band. The responsivity of optimized GaAs HIWIP detectors could be as high as 6 A/W, which is also much higher than QWIPs (edge coupled and grating coupled) and DWELL. Finally, by a very simple cavity design, which can be easily fabricated for practical applications, the performance of the p-GaAs HIWIP detector is further improved. A bottom gold layer is applied to serve as a BR for the device, which shows nearly 50% enhancement in responsivity compared with the device without BR. The resultant peak responsivity of the optimized p-GaAs HIWIP detector with BR could be as high as 6.8 A/W at 1 V. The NEP of 2.3×10^{-12} W/Hz$^{1/2}$ is demonstrated. Such a design method could be applied to the HIWIP detector operating at other peak frequency.

See supplementary material for the detection mechanism, the dark current mechanism, experimental details, and simulation results of the optical field distribution in the active region of the devices.

We acknowledge financial support from the Natural Science Foundation of China (91221201 and 11834011) and the Shanghai Sailing Program (17YF1429900). Peng Bai is thankful to Dr. T. M. Wang and Dr. J. Y. Jia for valuable discussions.

[1]A. Rogalski and F. Sizov, Opto-Electron. Rev. **19**(3), 346 (2011).
[2]I. Amenabar, F. Lopez, and A. Mendikute, J. Infrared Millimeter Terahertz Waves **34**(2), 152 (2013).
[3]H. Schneider and H. C. Liu, *Quantum Well Infrared Photodetectors: Physics and Applications* (Springer, Berlin, 2007).
[4]M. Graf, E. Dupont, H. Luo, S. Haffouz, Z. R. Wasilewski, A. J. S. Thorpe, D. Ban, and H. C. Liu, Infrared Phys. Technol. **52**(6), 289 (2009).
[5]M. Tonouchi, Nat. Photonics **1**(2), 97 (2007).
[6]S. Zhang, T. M. Wang, M. R. Hao, Y. Yang, Y. H. Zhang, W. Z. Shen, and H. C. Liu, J. Appl. Phys. **114**(19), 194507 (2013).
[7]R. Zhang, Z. L. Fu, L. L. Gu, X. G. Guo, and J. C. Cao, Appl. Phys. Lett. **105**(23), 231123 (2014).
[8]R. Zhang, X. G. Guo, C. Y. Song, M. Buchanan, Z. R. Wasilewski, J. C. Cao, and H. C. Liu, IEEE Electron Device Lett. **32**, 659 (2011).
[9]Y. N. Chen, Y. Todorov, B. Askenazi, A. Vasanelli, G. Biasiol, R. Colombelli, and C. Sirtori, Appl. Phys. Lett. **104**, 031113 (2014).
[10]D. Palaferri, Y. Todorov, Y. N. Chen, J. Madeo, A. Vasanelli, L. H. Li, A. G. Davies, E. H. Linfield, and C. Sirtori, Appl. Phys. Lett. **106**(16), 161102 (2015).
[11]S. Wolde, Y. F. Lao, A. G. U. Perera, Y. H. Zhang, T. M. Wang, J. O. Kim, T. S. Sandy, Z. B. Tian, and S. Krishna, Appl. Phys. Lett. **105**(15), 151107 (2014).
[12]A. G. U. Perera, H. X. Yuan, and M. H. Francombe, J. Appl. Phys. **77**(2), 915 (1995).
[13]A. G. U. Perera, H. X. Yuan, S. K. Gamage, W. Z. Shen, M. H. Francombe, H. C. Liu, M. Buchanan, and W. J. Schaff, J. Appl. Phys. **81**(7), 3316 (1997).
[14]W. Z. Shen, A. G. Unil Perera, M. H. Francombe, H. C. Liu, M. Buchanan, and W. J. Schaff, IEEE Trans. Electron Devices **45**(8), 1671 (1998).
[15]A. G. U. Pereraa, G. Ariyawansaa, P. V. V. Jayaweeraa, S. G. Matsika, M. Buchananb, and H. C. Liu, Microelectron. J. **39**(3), 601 (2008).
[16]H. X. Yuan and A. G. U. Perera, Appl. Phys. Lett. **66**(17), 2262 (1995).
[17]W. Z. Shen, A. G. U. Perera, H. C. Liu, M. Buchanan, and W. J. Schaff, Appl. Phys. Lett. **71**(18), 2677 (1997).
[18]M. M. Zheng, Y. H. Zhang, and W. Z. Shen, J. Appl. Phys. **105**(8), 084515 (2009).
[19]Y. H. Zhang, H. T. Luo, and W. Z. Shen, Appl. Phys. Lett. **82**(7), 1129 (2003).
[20]A. G. U. Perera, S. G. Matsik, M. B. M. Rinzan, A. Weerasekara, M. Alevli, H. C. Liu, M. Buchanan, B. Zvonkov, and V. Gavrilenko, Infrared Phys. Technol. **44**(5), 347 (2003).
[21]G. Yu, Y. H. Zhang, and W. Z. Shen, Appl. Surf. Sci. **199**(1), 160 (2002).
[22]Y. F. Lao, A. G. U. Perera, H. L. Wang, J. H. Zhao, Y. J. Jin, and D. H. Zhang, J. Appl. Phys. **119**(10), 105304 (2016).
[23]J. S. Blakemore, J. Appl. Phys. **53**(10), R123 (1982).
[24]W. Z. Shen and A. G. U. Perera, IEEE Trans. Electron Devices **46**(4), 811–814 (1999).
[25]A. Shen, H. C. Liu, M. Gao, E. Dupont, M. Buchanan, J. Ehret, G. J. Brown, and F. Szmulowicz, Appl. Phys. Lett. **77**(15), 2400 (2000).
[26]L. K. Wu and W. Z. Shen, J. Appl. Phys. **100**(4), 044508 (2006).
[27]Z. L. Fu, L. L. Gu, X. G. Guo, Z. Y. Tan, W. J. Wan, T. Zhou, D. X. Shao, R. Zhang, and J. C. Cao, Sci. Rep. **6**, 25383 (2016).